Journal of Physics: Conference Series **591** (2015) 012021 doi:10.1088/1742-6596/591/1/012021

Dense Plasma Focus – From Alternative Fusion Source to Versatile High Energy Density Plasma Source for Plasma Nanotechnology

R S Rawat[1]
Natural Sciences and Science Education, National Institute of Education
Nanyang Technological University, 1 Nanyang Walk, Singapore 637616

E-mail: rajdeep.rawat@nie.edu.sg

Abstract. The dense plasma focus (DPF), a coaxial plasma gun, utilizes pulsed high current electrical discharge to heat and compress the plasma to very high density and temperature with energy densities in the range of $1\text{-}10\times10^{10}$ J/m^3. The DPF device has always been in the company of several alternative magnetic fusion devices as it produces intense fusion neutrons. Several experiments conducted on many different DPF devices ranging over several order of storage energy have demonstrated that at higher storage energy the neutron production does not follow I^4 scaling laws and deteriorate significantly raising concern about the device's capability and relevance for fusion energy. On the other hand, the high energy density pinch plasma in DPF device makes it a multiple radiation source of ions, electron, soft and hard x-rays, and neutrons, making it useful for several applications in many different fields such as lithography, radiography, imaging, activation analysis, radioisotopes production etc. Being a source of hot dense plasma, strong shockwave, intense energetic beams and radiation, etc, the DPF device, additionally, shows tremendous potential for applications in plasma nanoscience and plasma nanotechnology. In the present paper, the key features of plasma focus device are critically discussed to understand the novelties and opportunities that this device offers in processing and synthesis of nanophase materials using, both, the top-down and bottom-up approach. The results of recent key experimental investigations performed on (i) the processing and modification of bulk target substrates for phase change, surface reconstruction and nanostructurization, (ii) the nanostructurization of PLD grown magnetic thin films, and (iii) direct synthesis of nanostructured (nanowire, nanosheets and nanoflowers) materials using anode target material ablation, ablated plasma and background reactive gas based synthesis and purely gas phase synthesis of various different types of nanostructured materials using DPF device will discussed to establish this device as versatile tool for plasma nanotechnology.

1. Introduction

The dense plasma focus (DPF) device was independently developed in variant forms by Mather [1] in the U.S. and by Filippov *et al.* [2] in erstwhile the U.S.S.R. during the 1960s. The DPF device basically consists of a fast discharging energy storage capacitor bank connected to the coaxial electrode plasma focus load in a vacuum chamber through a low inductance fast switch. The typical DPF operation involves: (i) the initiation of a powerful electrical discharge across an insulator at the closed end of a coaxial electrode system in focus chamber filled with operating gas typically at few mbar pressure, (ii)

[1] To whom any correspondence should be addressed.

followed by a current sheath formation and acceleration in axial phase toward the open end of the electrode assembly, (iii) rapid compression of current sheath at the top of the central electrode in radial collapse phase to form dense (~10^{26} cm^{-3}) and hot (~1 keV) pinch plasma column and (iv) finally the disruption and decay of pinched plasma column. Almost immediately after its development in 1960s, it was realised that the DPF is an abundant source of multiple radiations like neutrons, relativistic electrons, soft/hard X-rays, and fast ions but much of the initial interest and progress in DPF devices was driven by its high neutron yield.

1.1 DPF for Mainstream Fusion Research

During 1960s, the observation of highly intense burst of neutrons from DPF led to the premature announcement of thermonuclear fusion being achieved. As a result of this, research on DPF started in many laboratories [3-8] all over the world leading to great progress in improving the associated technology and in understanding of physical phenomena taking place in this system. The scope of DPF in fusion research increased as technological development enabled successful operation of large DPF machines leading to better understanding and formulation of scaling laws of DPF performances. Some of the main investigations concerning the scope of DPF in fusion research program are presented next.

The neutron yield in plasma focus device has been reported to scale as $Y_n \sim E_0^2$ where E_0 is storage energy of the DPF capacitor bank [9-12]. This led to the construction of bigger DPF devices with larger storage energy for higher neutron yields. Rager [13] proposed that a 30 MJ plasma focus facility, working much below breakeven at a level at which α-particles do no influence as yet the scaling of neutron yield and the plasma dynamics, may act as a nuclear design test facility as the achievable neutron fluence in this facility will be sufficiently high. He predicted that a 300 MJ facility may act as breakeven plasma focus for thermonuclear fusion application with product $n\tau = 3 \times 10^{20}$ $m^{-3}s$, neutron yield of about $Y_n = 3 \times 10^{20}$ neutron/pulse and thermonuclear power of 1 GW for 1 Hz repetition rate operation. Korzhavin [14] concluded that DPF of 30 MJ storage energy with 30 kV capacitor charging voltage will be energetically close to the thermonuclear efficiency of 10%. He argued, if the efficiency is further increased then the DPF neutron source will be able to produce the fuel for several reactor-convertors. It is well known that the neutron production in DPF devices is by joint thermal and beam-target acceleration mechanisms and the beam-target type collisions associated with instabilities are more dominant in comparison to thermonuclear reactions. Korzhavin [14] proposed that if the discharge current in DPF is raised to ten mega ampere then neutron emission will be purely thermal in nature with negligible contribution from turbulent mechanism. Gratton *et al.* [15] studied the properties of the out flowing corona generated by the ablation of solid micro sphere within a hot, dense plasma and noticed that plasma columns such as those produced in DPF devices may drive the implosion of the solid microsphere. They showed that the pinch plasma column of kJ DPF device is potentially a driver comparable to a multi-beam kJ Nd-Yag laser facility concluding that the attention should be paid to DPF research in context of inertial fusion research.

Experiments conducted in various labs on DPFs with different storage energy invariably observed and reported strong anisotropy in neutrons measurements with number of neutrons along the electrode axis to be always much higher than in the perpendicular direction suggesting that neutrons are mainly produced by beam target mechanism and contribution of thermonuclear origin is rather low [3, 16-20]. This resulted in serious doubts about the originally envisioned potentiality of DPF as an alternative thermonuclear fusion reactor. Nevertheless, the scope of DPF of in mainstream fusion research and technology was recognized as early as in late seventies when Cloth and Conrads [21] and Zucker *et al.* [22] proposed a programme to develop DPF as neutron source for blanket and materials problems of controlled thermonuclear reactor. It is a well-established fact that one of the key issues still to be resolved in the quest for fusion energy production is the characterization, qualification and development of advanced plasma facing materials capable of withstanding the extreme radiation and heat loads expected in fusion reactors from high flux of neutrons in addition to a plasma containing energetic gammas, x-rays, ions and electrons. The DPF is an excellent plasma simulator for testing materials under extreme conditions as it provides a realistic fusion reactor environment including

gamma rays, x-rays, ions, electrons and neutrons. The DPF is more energy efficient than most fusion plasma simulators because of the approximate E_0^2 scaling of neutron yield and the point source characteristics. It is accepted that large area reactor simulators would, no doubt, be necessary for screening of large number of materials, however, for specific material tests and to qualify the results of large scale fission reactor irradiations the DPF represents a good alternative. The advantages of DPF are high neutron yield with right neutron energy spectra, point source characteristics and possibility of higher repetition rate operations which allows high flux levels for faster tests or higher doses in reasonable time, relatively small size and cost and the lower power requirement. It is due to these reason the research efforts in this direction have continued and have recently gained more momentum through IAEA led coordinated research projects. IAEA has recognized and clearly stated in its report [23] that "*Dense magnetized plasma (DMP) devices serve as a first test bench for testing of fusion relevant plasma facing materials, diagnostic development and calibration, technologies and scaling to conceptual principles of larger devices while sophisticated testing facilities such as the International Fusion Materials Irradiation Facility (IFMIF) are being designed.*"

The concentrated and collaborative research efforts under the umbrella of IAEA's coordinated research project [24] is ongoing and expected to create (i) a data base of erosion rates of selected candidate materials (different tungsten grades and coatings, beryllium, CFC, SiC) under different heat and particle load conditions and different sample treatment scenarios and (ii) scientific base for improved understanding of mechanisms of plasma-material interaction and surface modification, possibly leading to the development of more advanced plasma-facing materials for fusion and other applications. While coming years will see the increased reporting of the research efforts and outcomes in this field this review is going to concentrate on another important development of the use and application of DPF devices for plasma nanotechnology.

1.2 DPF for Plasma Nanotechnology

The hot dense pinch plasma and plasma instabilities in DPF device makes it not only an intense source of fusion relevant neutron but also and an intrinsic, energetic and abundant source of multiple radiations like relativistic electrons [25-27], soft/hard X-rays [28-32], and fast ions [33-38]. These multiple radiations make it suitable for applications in wide variety of fields such as: pulsed activation analysis [39, 40], production of highly ionized species [41], X-ray lithography [42-48], X-ray radiography[49-57], and short lived radioisotope production [58-62]. In addition to the above mentioned wide ranging applications, another most regularly and routinely investigated application of DPF device has been in the areas of bulk and thin film material processing and synthesis. The first ever application of DPF device for processing of bulk material (AISI 304 stainless steel coupons) was reported by Feugeas *et al.* [63] while Rawat *et al.* [64] were first to report the processing of lead zirconate titanate thin film in DPF device. The first ever deposition of thin film, of carbon, was reported by Kant *et al.* [65]. After that more than hundred research papers have been written on various material processing and synthesis related work done by various plasma focus groups across the globe. Many of these papers highlight that in both cases, i.e. in case of processing of bulk substrates and thin films and also in case of direct synthesis of thin films, nanostructured materials are formed.

This review paper aims (i) to highlight several key and distinctive features of DPF device which sets it apart from routinely used low temperature plasma devices for nanostructured material synthesis, and (ii) to establish DPF as a novel high energy density plasma processing as well as deposition facility, in the fast emerging field of "Plasma Nanotechnology", for nanoscale material fabrications.

2. Plasmas for Nanoscience and Nanotechnology: Plasma Nanotechnology

The nanotechnology refers to the manipulation of matter with at least one dimension sized from 1 to 100 nanometers, through certain chemical and/or physical processes, to create materials, devices, and systems with fundamentally new properties and functions because of their small dimensions. The functionalization of nanoscale materials and their integration into nano-devices is leading to a revolution in wide ranging industries with numerous nanotechnology-enabled products fast becoming

part of our daily life. The conceptualization, development and optimization of various possible routes and processes, for synthesis of nanoscale materials, are one of the most active areas of research in nanotechnology. There are numerous routes for nanoscale material synthesis, which include milling and vapor condensation routes, chemical routes and nature's biological routes. The plasmas based and plasma-assisted processes have become most versatile tools of nanoscale fabrication as plasmas provide a complex, reactive and far from equilibrium chemical factory. This has led to the development of new field which is popularly referred as "Plasma Nanoscience" and/or "Plasma Nanotechnology" [66, 67].

The plasmas used in plasma nanotechnology can be broadly classified into (i) low temperature (cold) plasmas which are used by industry and material research community, and (ii) high temperature (hot) high energy density plasmas from fusion, pinch and intense discharge sources with densities and temperatures many orders of magnitude higher than that of cold plasmas. The following subsections provide key features of low and high temperature plasmas used in plasma nanotechnology.

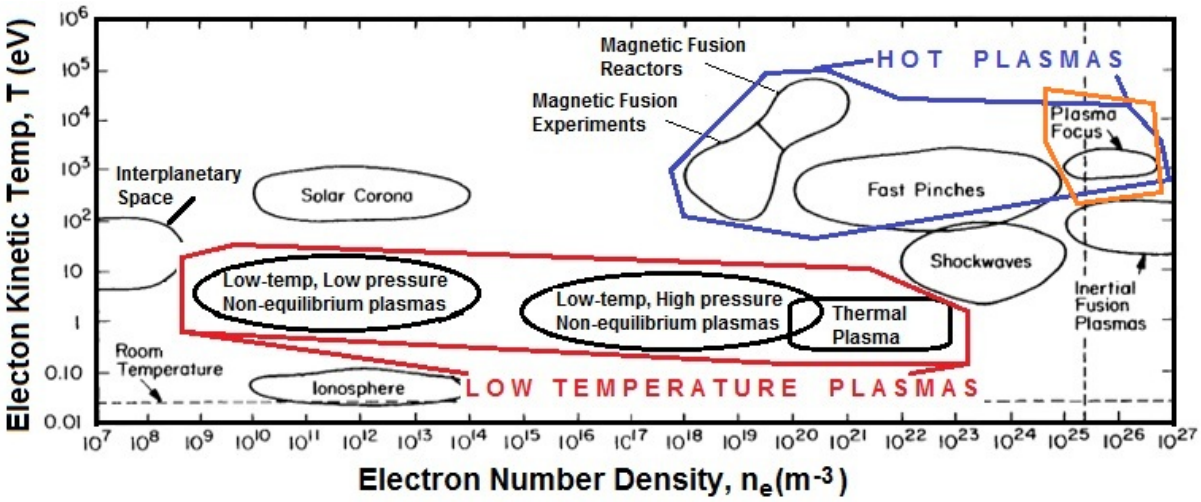

Figure 1. The plasma parameters of various types of plasmas. The low temperature plasmas routinely used in plasma nanotechnology are inside the red box while the high energy density DPF source is shown orange and blue box which belong to the category of hot plasmas.

2.1. Low Temperature (Cold) Plasmas for Plasma Nanotechnology

The low temperature plasmas are mainly produced by ac or dc electric gas discharge or by gas discharges initiated by RF or microwave electromagnetic fields and are characterized by low electron kinetic temperatures ranging from fractions to few tens of eV with low degree of gas ionization resulting in large fraction of the gas in neutral state. The low temperature plasmas used in plasma nanotechnology are grouped in red box in Figure 1 and can be further classified into non-equilibrium and equilibrium (thermal) plasmas. The non-equilibrium plasmas are formed when either the low operating pressure results in insufficient collisions between electrons and ions and neutrals and hence the equilibrium is not reached or high operating pressure having higher collision rates but the plasmas are short lived interrupting the equilibration process. They are described by relation $T_e >> T_i = T_g$, where T_e, T_i and T_g are temperatures of electrons, ions and background gas, respectively, and represent their mean kinetic energies. The thermal plasmas, on the other hand, are the plasmas in thermal equilibrium where the frequent collision between the electrons and ions and neutrals, for high pressure plasma discharges, results in equilibration of temperatures among the charged and neutral species i.e. $T_e \sim T_i \sim T_g$. The low temperature, equilibrium and non-equilibrium type, cold plasmas have been used extensively in plasma nanotechnology due to their interesting combination of electrical, thermal and chemical properties making them indispensable and versatile tool for plasma nanotechnology. The

excellent reviews and reports on various types of low temperature plasma that are used in plasma nanotechnology can be found in references [67-69].

2.2. High Energy Density High Temperature (Hot) Plasmas for Plasma Nanotechnology

The hot plasmas, grouped in blue box in Figure 1, have temperatures from few to several keV making matter to be in almost fully-ionized state. In this group of hot plasmas one can find the DPF device, focus of this review paper, on almost the highest side of plasma density. The energy density of DPF devices, estimated by dividing the energy stored in the DPF capacitor bank by the volume of the final pinch plasma column, is reported to be in the range of $(1.2\text{-}9.5)\times10^{10}$ J/m^3 [70] making it a high energy density plasma facility. The high energy density plasmas, by definition, refers to the plasmas which are heated and compressed to extreme energy densities, exceeding 10^{11} J/m^3 (the energy density of a hydrogen molecule) [71]. The magnitude of physical parameters associated with high-energy-density physics is enormous: shock waves at hundreds of km/s (approaching a million km per hour), temperatures of millions of degrees, and pressures that exceeds 100 million atmospheres. The plasmas with energy densities in the range of $(1\text{-}10)\times10^{10}$ J/m^3 are also now classified as high energy density plasmas and hence the DPF devices fall in this category. The Figure 1 shows the clear differences, in terms of plasma parameters, between routinely used low temperature plasmas in plasma nanotechnology and high energy density DPF device plasmas which are emerging as novel plasma nanotechnology tool with both plasma densities and temperature to be about minimum of two to three orders of magnitude higher than low temperature plasmas. It is not only the plasma temperature and the plasma density that are different in DPF devices compared to low temperatures plasma devices but there are several other features that uniquely belong to DPF devices and set them significantly apart from conventionally used low temperature plasma nanotechnology devices. These features are discussed next.

3. DPF: Device Layout, Plasma Dynamics and Key Features

The overall experimental setup of DPF device, with its main subsystems, as a material processing and deposition facility is shown in Figure 2. The DPF processing/deposition facility consist of (i) the DPF vacuum chamber containing (a) the coaxial electrode assembly consisting of central electrode (anode) surrounded coaxially by multiple cathode rods, (b) an aperture assembly, (c) a shutter, and (d) an axially moveable substrate holder; (ii) the vacuum pump and gas inlet connections; (iii) a capacitor bank connected to high voltage power supply; (iv) low inductance high current fast discharging switch (or switches) and transmission lines between the capacitor bank and the DPF load; (v) trigger electronics to activate the high current switches; and (vi) various diagnostics as per the requirements of the experiment being conducted.

The capacitor bank is first charged to high voltages (typically in 10-30 kV range) using high voltage power supply. The electrical energy stored in the capacitor bank is then transferred across the electrode assembly by activating fast switches which initiates a discharge across the insulator sleeve at the closed end of the electrode assembly. This discharge then evolves into a well-defined sheath of plasma in about 100 to 500 ns for DPF devices having the quarter time period of about 500 and 3000 ns, respectively [32, 72]. The current sheath then moves in an inverse pinch manner forming an axially symmetric current sheath near the closed end of the electrode assembly. Driven by $\mathbf{J}\times\mathbf{B}$ force, the current sheath then accelerates along the electrode assembly in what is commonly referred as axial acceleration phase. The typical current sheath speed in axial acceleration phase is reported to be about 4-6 cm/μs. As the current sheath reaches the open end of the anode and starts to roll over anode it is said to enter into radial acceleration phase where it collapses on anode axis forming the hot and dense pinch plasma column. The radial speed of current sheath in radial compression phase is about 2 to 2.5 time the speed in axial phase which results in extremely fast moving shock. The fast moving shock front ahead of the collapsing current sheath can result into plasma temperature of about several hundred electron volts; while the reflected shock at the axis, together with the magnetic compression, can finally raise this temperature to around 1-2 keV. Soon after the formation of pinched plasma

columns it breaks up due to $m = 0$ and $m = 1$ instabilities. The $m = 0$ mode instabilities accelerate the ions of the filling gas species to very high energies towards the top of the chamber and accelerate electrons to relativistic energies (100 keV and above) towards the positively charged anode. A fast moving axial ionization wave-front, produced by the ionization caused by energetic ions, later develops into a bubble-like structure [73]. The ionizing front coincides with the beginning of the hard X-ray emission due to the interaction of energetic electron with anode tip material and also the neutron pulses for deuterium filled DPF device. The pinched plasma column finally breaks up and disintegrates leading to the decay of hot and dense plasma. For more details about DPF devices readers are advised to refer to excellent reviews written by J. Tendys [8], A. Bernard *et al.* [74], V. A. Gribkov *et al.* [56], and M. Krishnan [12]. A detailed review highlighting several applications of DPF device in plasma nanotechnology can also be found in reference [75].

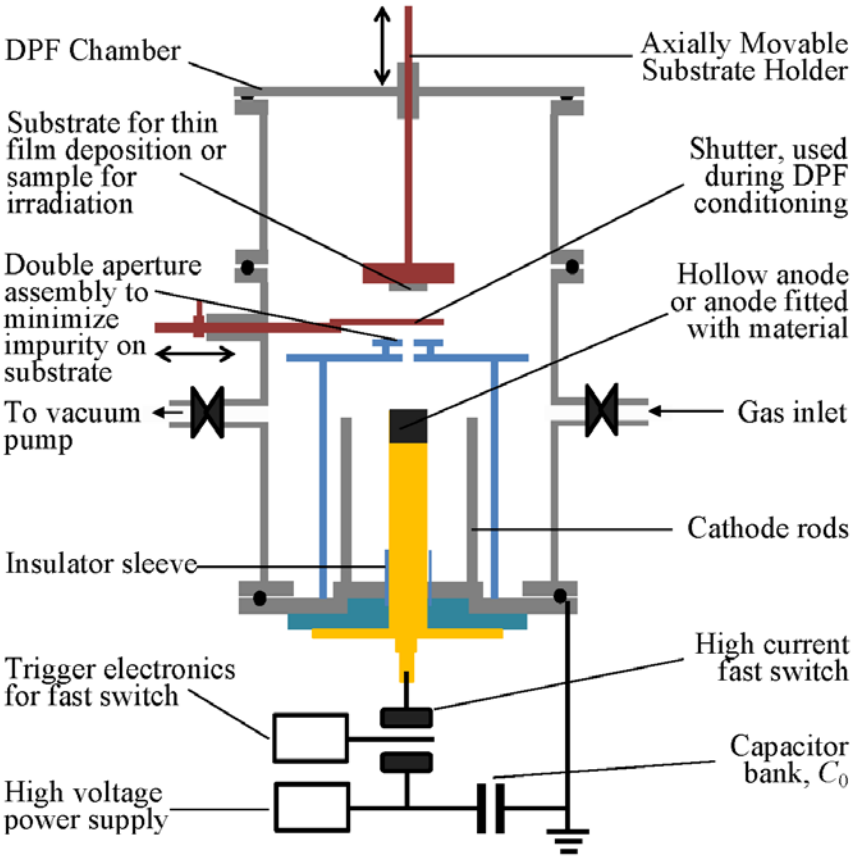

Figure 2. The schematic of DPF material processing/synthesis facility with its various subsystems.

The optimized DPF devices exhibit unique universality i.e. many typical parameters and characteristic features of pinch plasmas, current sheath dynamics, various radiation and energetic charged particles are very similar and are not affected by the dimensions of coaxial electrode assembly, capacitor bank energy, peak discharge current, and the operating gas type. The typical values of various key parameters of interest for optimized DPF devices that exhibit unique universality of DPF devices are given below.

(i) The current sheath speed in axial acceleration phase is typically in the range of 2 to 10 cm/μs [9, 76] which shock-heats the plasmas to electron and ion temperatures of about 100 and 300 eV, respectively, at the end of the axial acceleration phase [77].

(ii) The current sheath speed in radial compression phase is typically about 2 to 2.5 times that of the axial speed [76].
(iii) The electron/ion densities in pinch plasmas are in the range of 5×10^{24} –10^{26} m^{-3} [37, 78].
(iv) The electron and ion temperatures of pinch plasmas are in the range of 200 eV – 2 keV [73] and 300 eV – 1.5 keV [78], respectively.
(v) The energies of instability accelerated electrons, which moves towards the anode, are in the range of few tens to few hundreds of keV [25, 79].
(vi) The energies of instability accelerated ions, which mostly move axial along the anode axis towards the top of the DPF chamber, are in the range of tens of keV to few MeV [33, 80]. The ions are mostly forward directed with most of the ions being emitted in narrow angel of 20° with respect to the anode axis.
(vii) The UV, soft and hard x-rays with photon energies ranging from hundreds to several hundred thousands of eV have been measured in DPF device [28-32].

The DPF devices are essentially transient discharge of a capacitive driver, C_0, into an inductive load, L comprising of fixed system inductance L_0 and dynamic plasma inductance L_p, with the characteristic transient discharge duration of the order of the $\sqrt{LC_0}$, which typically ranges from few hundred ns for low energy sub-kJ DPF devices to several μs for high energy hundreds of kJ or MJ large DPF devices. Hence the durations of pinch plasma, radiation and energetic particles in DPF devices, which are typically some fraction of characteristic discharge duration, are of the order of tens of ns to about hundred or several hundred ns [50 – 53]. *This makes all phenomena of interest in DPF device being highly transient in nature.* Hence, "*in DPF devices the very high densities and temperatures of pinch plasmas, very high flux of high energy instability accelerated ions and electrons, intense energetic radiations, fast moving shock and hot-dense decaying plasma combined with their transient nature offers a kind of plasma and radiation environment that is drastically different from the ambience of low temperature plasmas conventionally used in plasma nanotechnology for nanostructured material synthesis*".

4. Top-down and Bottom-up Nanoscale Fabrications using DPF devices

The nanostructured material synthesis methods involve two different strategies commonly referred as "bottom-up" and "top-down" approaches, shown in Figure 3. The "bottom-up" approach creates nanoscale materials from assembling atoms and molecules; while the "top-down" approach relies on the successive fragmentations or processing of macro-scale materials to smaller nano-sized objects. The radiation and charged particle emission characteristics of DPF allow the nanostructured material synthesis through both routes.

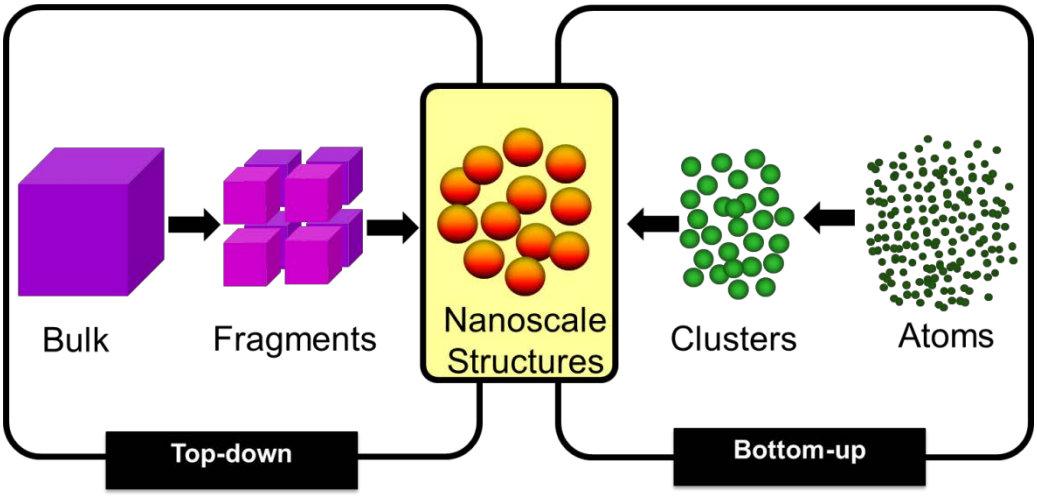

Figure 3. "Top-down" and "bottom-up" synthesis of nanofabrication.

4.1. Top-down Nanoscale Fabrication by Transient Processing of Bulk/Thin Films in DPF

This method involves the exposure of bulk or thin film samples to the different number of DPF shots. It may be pointed out that while the nanostructurization of the entire thickness of the thin film can be achieved by its exposure to DPF shots but for bulk material only the top surface layer of the bulk sample is processed and nanostructurized by its exposure to DPF shots. The setup for the processing of bulk or thin film sample in UNU-ICPT DPF facility, which is a 3.3 kJ device at 15 kV charging voltage with peak discharge current of about 170 kA, in our Plasma Radiation Source Lab in Nanyang Technological University, Singapore is shown in Figure 2. The sample, to be processed, can be placed either along the anode axis or different angular position with respect to the anode axis and at different distances using an axially moving sample holder

The sample exposed to DPF shot is processed by a complex mix of high energy high-flux photons, instability accelerated energetic ions, fast moving ionization wave-front, strong shock wave, and hot and dense decaying plasma. For efficient processing of samples in DPF device one should take note of following additional characteristics of DPF device and use the appropriate strategies:

(i) The DPF devices possess a point-source like characteristics and therefore it can be safely assumed that the above mentioned energetic ions, radiation and hot-dense decaying plasma are essentially emitted from point source (tip of pinched plasma column) and then spread out. Hence, with the increasing distance of exposure the ions/radiation/plasma flux will decrease or in words the energy flux delivered at different distances of exposure is different. This gives the possibility of different degree of processing of the sample by simply changing its exposure distance from the anode top and also by using different number of DPF exposure shots.

(ii) One of the drawbacks of DPF devices is the lack of exact reproducibility i.e. there is variation in device performance (and hence the radiation and charged particle yield) from one shot to another. To minimize the shot to shot variation in performance the device should be conditioned for consistent and efficient performance. Normally, few to few tens of conditioning shots are required, depending on device and its prior state of operation, to achieve efficient pinching in DPF device. During conditioning shots a mechanical shutter should be employed, refer Figure 2, to avoid any unwarranted exposure of sample to the less efficient conditioning shots. The conditioning of DPF ensures reliable shot to shot operation of DPF device. Once the good focusing efficiency, monitored by current and/or voltage probe, is achieved then the shutter is removed and the sample is exposed during the next DPF shot.

(iii) Another important area of concern for irradiation/processing experiments in DPF is the metal impurities from ablation of anode material by the instability accelerated electrons and hot dense pinch plasma. If substantial care is not taken then undesirable debris of ablated anode top material may deposit on the exposed sample surface. The ablation on undesirable anode material can be minimized, to a very large extent, by using deep hollow anode with relatively thin wall. A further reduction in anode wall material debris on the exposed sample surface is achieved with the use of aperture assembly, shown in Figure 2. The aperture assembly should preferably be made up of material which has higher ablation threshold such as brass.

(iv) Depending on the application, one should carefully choose the gas to be used as the operating media. Inert gases such as neon and argon have been used in many studies where the aim was to simply process the material to change its physical characteristics without affecting its composition. Reactive gases such nitrogen, oxygen, acetylene, methane etc. have been used for the formation of nitrides, oxides and carbides in the irradiated/processed materials.

(v) Due to delivery of high flux and high energy instability accelerated ions, energetic radiations, shock exposure and hot-dense decay plasmas in a very short time (with different events lasting from few tens of ns to several μs), the processing of material in DPF device is equivalent to ultra-fast annealing. Sanchez and Feugeas [81] estimated the generation of intense transient heating slopes and heating speeds as high as ~3600 K μm^{-1} and ~40 K ns^{-1} respectively, on various metal sample surface confirming the ultra-fast annealing rate in DPF device. The rapid surface temperature rise, beyond evaporation point, followed by the rapid cooling results in

strong thermal effect on the exposed material which bring out the changes in their several physical properties and compositional characteristics. The extent of thermal excursion of the sample surface can be tailored easily either by changing the exposure distance or the angular position of the sample being exposed.

It may be important to highlight over here that though the processing of target material in DPF device is a very complex process due to the involvement of very complex radiation, shock and plasma wind but the main processing component undoubtedly is the forward-directed energetic ion beam. Typical characteristics of energetic ions have been mentioned earlier in section 3. The nano-structuring of thin film, through nanoparticle formation, using single DPF shot irradiation with hydrogen as the operating gas was firstly reported by Jiaji *et al.* [82]. To understand the mechanism of nanoparticle formation they used a Faraday cup and deduced H^+ ion energies to be in the range of about 35 keV to 1.5 MeV and ion flux to be about 2.63×10^{14} ions cm^{-2} at target placed at 5 cm from the anode top. As mentioned, for various processing and ion implantation experiments different gases such as argon, nitrogen, hydrogen, carbon etc. ions have been used in DPF devices. Recently, ion beam fluences and flux for various gases, at the exit point of the pinch, in a DPF device have been numerically estimated and reported by Lee and Saw [83, 84].

Following sub-subsections, using some selected examples, will illustrate the application of DPF device for nanoscale fabrication after being processed by transient complex mix of radiation, shock, plasma and charged particle.

4.1.1. Nano-structuring of Bulk Substrate Surface. Several experiments have conducted and reported on exposure of different bulk substrate materials, such as titanium [81, 85-90], stainless steel [63, 81, 91-93], silicon [94-100], aluminium [101-103], zirconium [104-110], zirconia [111], tungsten [112] etc, using plasma focus devices. Many of the SEM (scanning electron microscopy) images of the DPF irradiated sample surfaces shown in these research paper clearly show the surface reconstruction with nanostructures being formed on them. The formation of nanostructures on Ti and W samples exposed to different DPF devices for different number of shots, at different distances and angular positions, for different filling gas is shown in Figure 4. The surface of the unexposed Ti and W substrates are shown in Figure 4(a) and 4(g), respectively. The low-magnification image in Figure 4(a) shows linear scratch marks of mechanical polish on unexposed Ti sample surface by abrasive silicon carbide paper, while the high magnification image of unexposed W samples in Figure 4(g) shows variable sized and shaped grains and pits. The exposure of these bulk substrate samples to DPF shot with efficient pinching, as indicated by electrical probe signals, at lower distances of exposure causes extreme transient temperature rise of the top few micron thick layer of the sample surface which results in sputtering, melting and re-solidification of this top layer. This is clearly seen in Figure 4(b) which shows reconstruction with extensive smoothening of the exposed surface after the Ti sample, placed along anode axis at axial distance of 5 cm, is irradiated with 30 DPF shots with nitrogen as the operating gas. The SEM image at higher magnification, refer Figure 4(c), shows the formation of self-organized linear nanostructures on the sample surface. It may be mentioned that the dark grey islands observed in Figure 4(c) are not large grains but itself composed of very small nanoparticles (not visible at this magnification) within the boundaries of these linear nanostructures. The exposure of Ti substrate to DPF operation in nitrogen ambience led to the TiN layer formation on the substrate surface. The greater details about the structural, compositional and hardness of the surface TiN layer can be found in our paper [88].

Similarly, the exposure of Ti substrate to methane operated plasma focus devices led to formation of nancomposite titanium oxycarbide (TiC_xO_y) layer on the exposed Ti substrate surface where the carbon was provide by the dissociation of background reactive methane and oxygen probably came from the background impurity. The exposure of Ti substrate to methane operated DPF was conducted in two different DPF devices; low current 190 kA, 3.2 kJ single shot UNU/ICTP DPF and high performance 430 kA, 3.1 kJ NX2 DPF devices. The comparison of SEM images in Figure 4(d) and 4(f) shows the formation of titanium oxycarbide nanoparticles on the substrate surface for both DPF

devices exhibiting the reproducibility of the results from two independent devices. The reproducibility of results is one big question mark on the credibility of DPF device for material related work that the critics would often raise due to the well-known shot to shot variation of DPF devices. But our experience has demonstrated that for a vigorously optimised DPF device this is not an issue as the running average performance of a well optimized device can be very consistent [113]. The size of nanoparticles in Figure 4(d) is about 35-50 nm whereas in Figure 4(f) is about 20 nm. The bigger size of nanoparticles in Figure 4(d) is attributed to the higher energy and material flux due to exposure at lower distance as well as along the anode axis. The off-axis irradiation at angular position of 10° with respect to anode axis as well as at higher distance of 9 cm results in lower material and energy flux at the irradiated substrate surface leading to smaller nanoparticle size. The SEM image of the Ti substrate exposed along anode axis in NX2 device, shown in Figure 4(e), exhibits features similar to the one observed in Figure 4(c) with linear nanostructures. The greater details about the structural, compositional and hardness of the nanostructured nanocomposite titanium oxycarbide layer formed on DPF irradiated Ti substrate surface can be found in our paper [87].

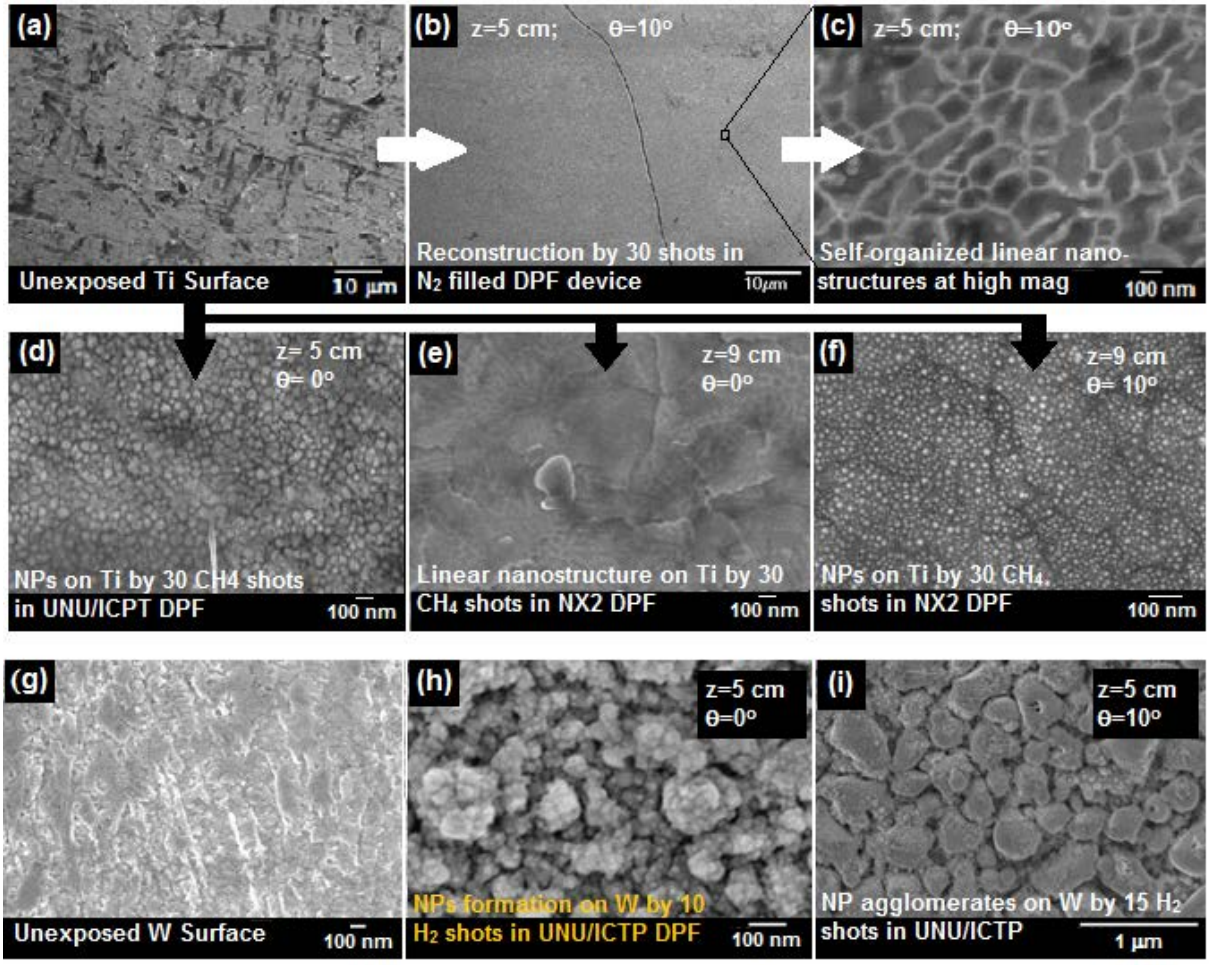

Figure 4. SEM images of unexposed and irradiated Ti and W samples in different DPF devices. The distance (z) and angular position (θ) of the samples, number of DPF irradiation shots and DPF operating gas for each of the exposure experiment are mentioned in SEM images.

The Figure 4(g-i) shows SEM images of the unexposed and irradiated tungsten samples. The unexposed mechanically polished sample in Figure 4(g) shows the rough surface but as such does not show any nanostructure formation. The SEM images of 10 and 15 shot irradiations in hydrogen

operated UNU/ICTP DPF device, shown in Figure 4(h) and 4(i) respectively, exhibit the formation of nanoparticles and nanoparticle agglomerates on the irradiated tungsten surface. The size of nanoparticles is about 15-20 nm for 10 shot irradiation though the nanoparticles are also seen to agglomerate resulting in the formation of particle agglomerates with size varying from 100 to 300 nm. The tungsten sample irradiated with 15 shots shows mostly particle agglomerates with the further increase in their size to about 200-800 nm. It may however be noted that these big size particle agglomerates are made up of nanoparticles with size varying from about 40 to 60 nm. The increase in nanoparticle and particle agglomerate size with greater number of irradiation shots can be attributed enhanced transient thermal treatment of the sample surface.

4.1.2. Nano-structuring of Thin/Thick Films. The nano-structuring of pulsed laser ablation deposited FePt thin films in hydrogen operated DPF device [82, 114, 115] and polyaniline thick film in nitrogen operated DPF device [116] has been demonstrated. The FePt thin films were processed in main DPF chamber essentially by upwardly moving hydrogen ions as the aperture assembly was used whereas the polyaniline (PA) thick films were processed by backward moving relativistic electron beam after being extracted through the hollow anode in a separate chamber attached to bottom exit point of the anode as shown in Figure 5. The FePt thin films and PA thick films exposures were done in two different DPF devices and Figure 5 represents the combined schematic of the experimental setup of these two different experiments. The PLD grown 67 nm FePt samples were processed in 3 kJ hydrogen operated UNU-ICTP DPF device by Jiaji *et al.* [117] at a distance of the 5 cm from the anode top, while the few tens of micrometer thick PA films prepared by chemical oxidation method were exposed in 2.2 kJ Mather-type nitrogen operated DPF device [33] by Mohanty *et al.* [116].

The SEM images shown in Figure 5 show that the surface morphology of FePt thin films changed from smooth uniform film for as-deposited sample to the film with uniform and isolated nanoparticles after a single DPF shot exposure. The average size of the FePt nanoparticles formed upon single shot exposure was found to be about 9.1±2.3 nm. The increase in number of ion irradiation DPF shots to two resulted in agglomeration of FePt nanoparticles to bigger sized agglomerates of about 51.3±7.4 nm. Z.Y. Pan *et al.* repeated the experiments with 100 nm thick PLD grown FePt thin films and were able to reproduce nano-structuring of FePt thin films in hydrogen operated UNU-ICTP DPF device using different number of focus shots [114] as well as different exposure distances (5, 6 and 7 cm) [115]. The mechanism of nano-structuring of the DPF exposed thin film can be understood from the characteristics of instability accelerated ions of the filling gas species. Though the ion energy is found to vary over a very big range from few tens of keV to few MeV, but the mean energy of the bulk of the H^+ ions in UNU-ICTP DPF has been estimated to be 124 keV [82]. The projected range of the H^+ ions of this mean energy is about half-micrometer in FePt, as estimated from SRIM ®. Therefore, most of the H^+ ions stop and deposit bulk of their energy in silicon substrate at the Bragg peak position as the thickness of FePt thin films was only about 67 or 100 nm. This would result in heating of silicon substrate to very high temperature in a very short span of time. The thermal energy is then conducted to the FePt thin films and causes the diffusion of metal atoms either through the lattice or along grain boundaries. The diffusion releases the thermal expansion mismatch stresses between the silicon oxide layer of the silicon substrate surface and the PLD coated FePt thin film, leading to the formation of nanoparticles at the surface layer of FePt thin films. One of the biggest advantages of nano-structuring using a DPF device is that it can achieve nano-structuring of thin film in single shot exposure with ion pulse duration of the order of a few hundred ns compared with hours of irradiation time required for other reported continuous ion sources [118].

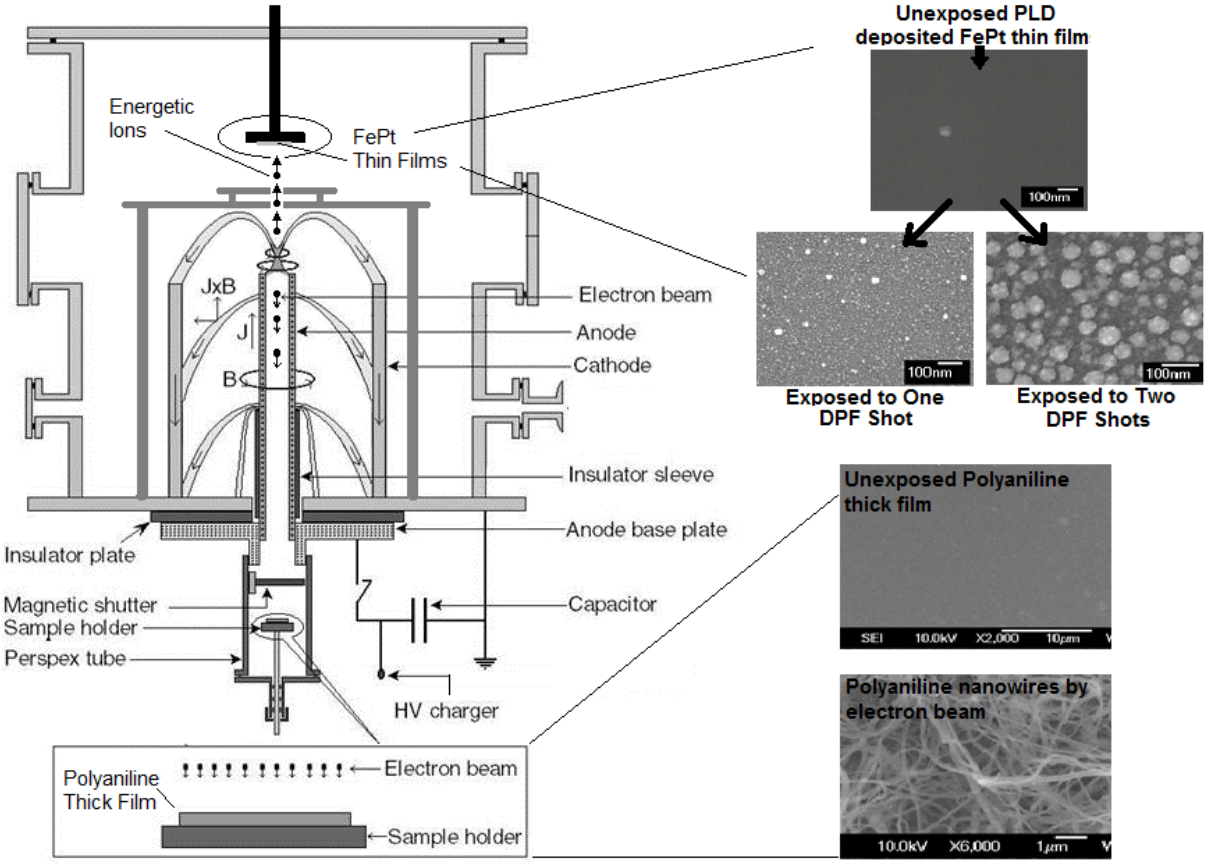

Figure 5. The combined schematic of DPF device showing the exposure of FePt thin film to energetic ions in UNU/ICTP device in Singapore [117] and PA thick film to energetic electrons in another DPF device in Guwahati, India [116]. The images on the right show the changes in surface morphology to nanoparticles and nanowires after DPF exposure.

The SEM images of the unexposed and energetic electron beam exposed PA films are also included in Figure 5. As-synthesized PA thick films are relatively smooth with some aggregates of polyaniline granules. Exposure of PA thick films to the electron beam in a single DPF shot resulted in the formation of network of interwoven nanowires, with diameter of about 50–80 nm and lengths extending up to 10 μm, at many places over the film sample surface, as shown in Figure 5. Liang *et al.* [119] took several hours for making PA nanowires using electrochemical deposition whereas Mohanty *et al.* [116] were able to grow network of PA nanowires in single DPF shot in ultrashort time-scale of about microsecond, the pulse duration of energetic electrons [120] in DPF device.

4.2. Bottom-up Nanoscale Fabrication in DPF

The DPF devices have been used for the deposition of different types of thin films [25, 65, 107, 110, 121-139]. It has invariably been observed that the surface morphologies of thin films deposited with DPF are essentially nanostructured with nanoparticles and nanoparticle agglomerates. Many different thin film deposition configurations, shown as setup C1 to setup C4 in Figure 6, have been used in DPF devices. Before moving on to discuss the bottom-up nanoscale fabrication in DPF device through some selected examples, the following subsection provides the details of different thin film deposition configurations that have been used in DPF devices.

4.2.1. Deposition Configurations of DPF Devices for Nanoscale Fabrication. The first ever configuration for thin film deposition in DPF device, used for carbon thin film synthesis by Kant *et al.*

[65], is shown as setup C1 in Figure 6. The setup C1 used the instability accelerated energetic ion beam and hot dense decaying plasma to ablate the target T placed down the anode stream in specially designed Perspex box in which the substrate was mounted in geometrical shadow region of the box to avoid its direct exposure to ions and plasma from the anode top. This setup used hollow anode to reduce impurities from anode rim to be deposited on the target. The method, however, has drawbacks of poor target ablation, deposition of anode material impurities on target, and ablation of Perspex box material by ions and hot-dense decay plasma resulting in more impurities.

One of the commonly used DPF based deposition configurations is the setup C2 where no substrate was used for thin film deposition rather the bulk target surface irradiated at lower distances gets sputtered, melted and re-solidified to form a top thin layer of different stoichiometry on the target itself. For example, when the targets T of materials such as Ti/Al/Zr/W etc. are exposed to DPF shots operated with reactive background gas such as nitrogen then the thin layer of TiN/AlN/ZrN/WN etc. are observed to form on target surface [86, 92, 105, 140, 141]. The operation of DPF with carbon containing gas such as methane or acetylene or combination of gases such methane and nitrogen has resulted in the formation of carbide [85, 97, 98, 142] or carbonitride [99, 108] thin films on the irradiated target surface. This method, though simple, has the disadvantage of thin film being not transferred to other substrate material and it is very difficult to find and control the thickness of the top layer formed. Moreover, these experiments were conducted mainly with hollow copper anode and would still have the probability of having ablated copper impurities to be deposited on the top layer.

The setup C3, shown in Figure 6 and first time used and reported by Rawat *et al.* [121], is the most flexible and versatile DPF based thin film deposition configuration whereby either the entire anode or anode tip is made of the target material (to save the cost) and the substrate (on which thin film is to be deposited) is placed at a certain fixed distance from the anode top either along the anode axis or at known angular position. A suitable (inert or reactive) operating gas and anode tip material combination is used for the deposition of various types of thin films on suitable substrate. For example, hard coating of TiN can be deposited on stainless steel (SS) substrate by using DPF fitted with Ti anode or Ti anode tip on copper anode and by operating the DPF in nitrogen ambience [122]. High pinch plasma temperature causes the complete ionization of the filling gas species (nitrogen) resulting formation of nitrogen ions, atoms and molecules. The interaction of backward moving relativistic electrons and energetic plasma cause the ablation of Ti anode material forming the Ti plasma which then reacts with ambient nitrogen plasma resulting in TiN formation on SS substrate placed down the anode axis. Similarly, for TiC coating the Ti anode fitted DPF just needs to be operated with gas containing carbon such as methane or acetylene. It has however been found that the DPF operation in these gases is non-reliable and inconsistent [121]. It is for this reason these gas are normally used as admixture with inert gases such as argon or neon. Thus, the deposition of thin films of carbides, nitrides or oxides of any metal can simply be achieved using suitable reactive background gases such nitrogen, acetylene, methane, and oxygen or their combinations. In case of synthesis of magnetic materials, such as Fe, FeCo, CoPt etc., reactive gases were not used rather the device was operated either in inert ambient or with hydrogen. The use of entire anode or the anode tip made up of the material which (or whose compound) is to be deposited on substrate removes anode impurity problem faced in the setup C1 and C2. The ablation rate of the target material is highest for the setup C3 resulting in higher deposition rates for this deposition configuration. As the depositions in DPF devices are conducted in multiple shots, the energetic ions of the filling gas species from next DPF shot process the material deposited in previous shot in a way similar to the one explained in setup C2. The setup C3, therefore, can be classified as *ion and plasma assisted pulsed electron deposition process* as the hot-dense decaying plasma and the energetic ions of gas species also process the thin film that is deposited on the substrate surface.

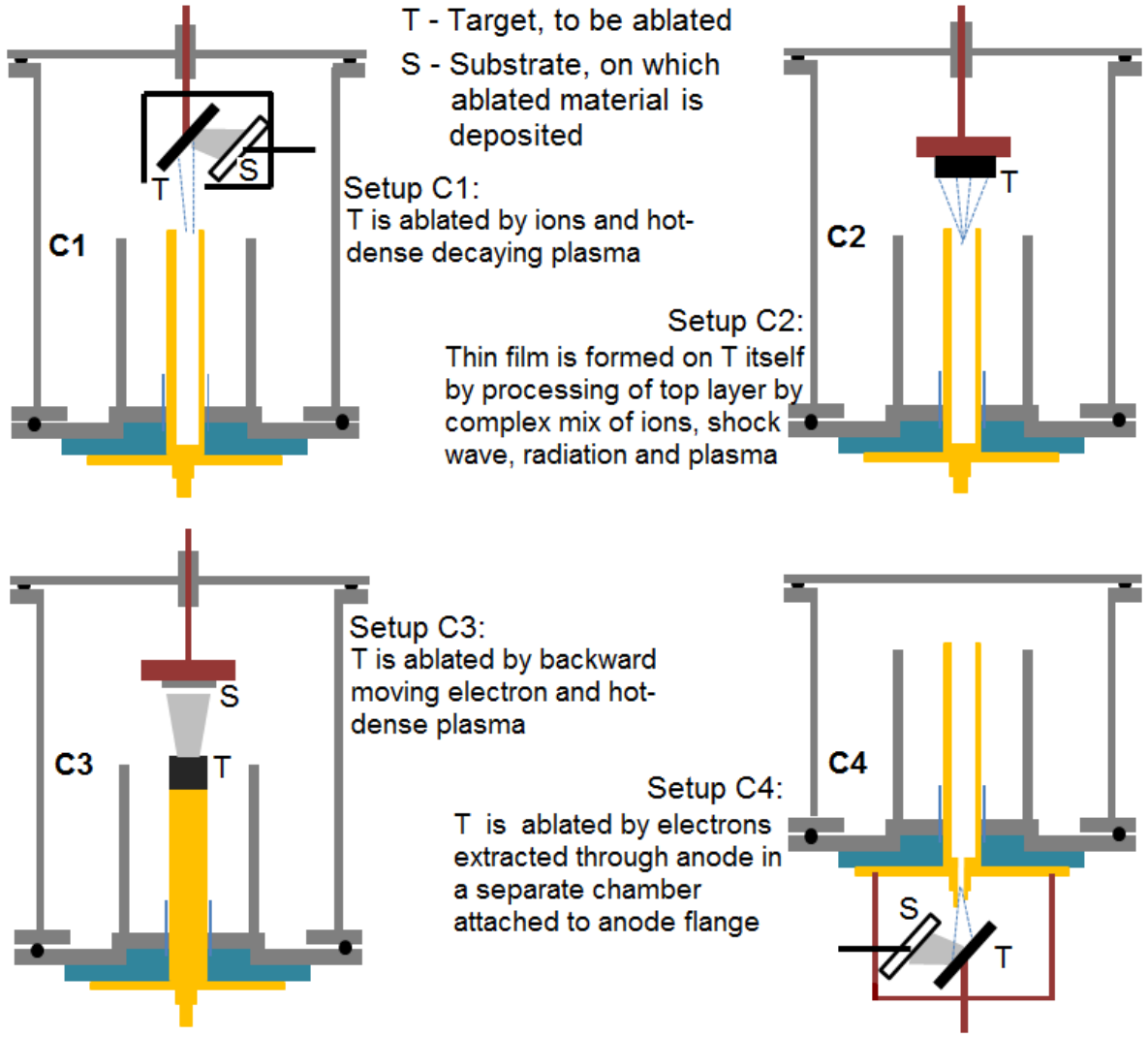

Figure 6. Various configurations of target (material to be ablated and deposited) and substrate in DPF devices used for thin film depositions. Different setups (C1 to C4) use different plasma/radiation components for target ablation.

The deposition configuration shown as setup C4 in Figure 6 was used Zhang *et al.* [25] for deposition of nanostructured thin film of FeCo. They referred their setup as PFPED (Plasma Focus assisted Pulsed Electron Deposition) facility in which an additional chamber was attached to the anode flange within which the ablation of the target material was essentially done by pulsed relativistic electron beam extracted through the hollow anode. The development of PFPED was motivated by the use of pulsed high power electron beams as novel tools for processing of material surfaces [143, 144] and their ability to exhibit stoichiometric deposition of complex multi-component materials [143, 145]. The routinely used deposition method of setup C3 has the advantage of efficient and effective ablation of anode material, however it also has disadvantages such as (i) the energetic ion bombardment of the deposited sample by the next deposition shot are inevitable, which may have a positive or a negative influence and also allows lesser control over the processing of the deposited material and (ii) the deposition chamber is always at high filling gas pressures (in the mbar range) compared with other plasma based deposition systems. The chamber pressure range in setups C1 to C3 is essentially controlled by mass number of filling gas species (bigger is the mass number and smaller is the pressure operation range of PF) etc. The PFPED of setup C4 provides much better control over

the deposition process in the PF device as the unavoidable exposure to energetic ions and plasmas is not there. On the other hand, the setup C4 is more difficult to assemble and the target ablation rate (and hence the thin film deposition rate) is much lower compared to setup C3.

Each of the DPF based deposition processes shown in setup C1 to C4 has its own limitations and disadvantages but based on the extensive experience that our group has we strongly believe that the setup C3 is the most versatile and efficient for thin film deposition. The next subsection, using some selected examples will illustrate key features that DPF offers in nanoscale fabrication or nanostructured thin film formation.

4.2.2. Selected Examples and Features of Nanoscale Fabrication using DPF Devices. The Figure 7 shows the some selected SEM images of nano-structured material synthesized using DPF devices. It can be seen from SEM images that DPF devices is able to synthesize 0-, 1-, 2- and 3- dimensional (dim) nanostructures. The spherical nanoparticles (NPs) seen in Figure 7(a-d) are the examples of 0-dim nanostructures that are the most routinely synthesized in DPF devices. While NPs are visibly present over the entire substrate surface in Figure 7(a & b), they are also present as the background in Figure 7(c & d). It was interesting to note that once background carpet of 0-dim NPs is formed on the substrate surface then higher dimensional nanostructures, such as 1-dim linear network of beaded NPs (seen in Figure 7(c)) and 2- and 3-dim nanostructures such as graphene nanosheets (features in white circle marked as 1 in Figure 7(d)) and graphene nanoflowers (features in green circle marked as 3 or 3G in Figure 7(d)), can grow on this NP carpet. It may be important to point out that the graphene nanosheets and nanoflowers are grown in gas phase synthesis by using methane-nitrogen admixture discharge in UNU/ICTP device. These are very new and exciting results where the DPF device has been successfully used for synthesis of 2- and 3-dim nanostructures and will be presented in detail in near future.

It has invariably been observed that the surface morphologies of thin films deposited with DPF are essentially nanostructured with NPs formed over the entire substrate area particularly when deposition setup C1, C3 and C4 (shown in Figure 6) are used. The synthesis mechanism of NPs in DPF device can be understood by drawing analogy from PLD based synthesis of NPs. Happy *et al.* [146] investigate the surface morphology of FeCo thin grown by PLD method. They observed smooth and uniform FeCo thin films formation on substrate surface, without any nanofeatures, at low background pressure operation (about 10^{-6} mbar) of PLD chamber. The low background pressure lowers the interaction of laser ablated plasma with background gas resulting in higher kinetic energy of the plume species on the substrate surface leading to greater adatom mobility and hence the uniform thin film formation on the surface. The high pressure operation (mbar range), according to them and Jiaji *et al.* [147] on the other hand, results in lower kinetic energy of the ablated species on the substrate surface leading to less adatom mobility on substrate surface resulting in NP formation. The DPF deposition setups of C1, C3 and C4 are similar to PLD with the difference that the target ablation, instead of being done by intense laser light, is caused different radiation/charged particle/plasma component. The DPF operation however is always limited to higher pressure regime, typically in the range of about few mbar for all gases, for efficient plasma focus operation. This leads to 0-dim NPs formation on the substrate surface, as explained above, in all DPF based depositions.

Other features of nanostructured material synthesis in DPF devices, as deduced from several experiments conducted and reported by different groups, are as follows:

(i) Until certain number of DPF deposition shots, the size of NPs increases with the increasing number of focus shots. The increase in NP size with the increase in number of shots is seen in image sequence (a) to (d) in Figure 8. The average size of FeCo NP was found to increase linearly from about 45 nm for 10 shots deposition to about 75 nm for 30 shots deposition in UNU/ICTP DPF device for depositions done at substrates angular position of 18° with respect of the anode axis [126]. The increase in NPs size with the increasing number of deposition shots is also observed at higher angular position of 36°. This implies the NPs synthesized and

deposited during the first DPF shot continue to act as the growth site resulting in increase in NP size with more shots. However, as mentioned earlier through the observation in Figure 7 that after certain number of DPF shots, depending on the nature of material being deposited, higher dimensional nanostructures may start to nucleate/grow on background NPs carpet layer.

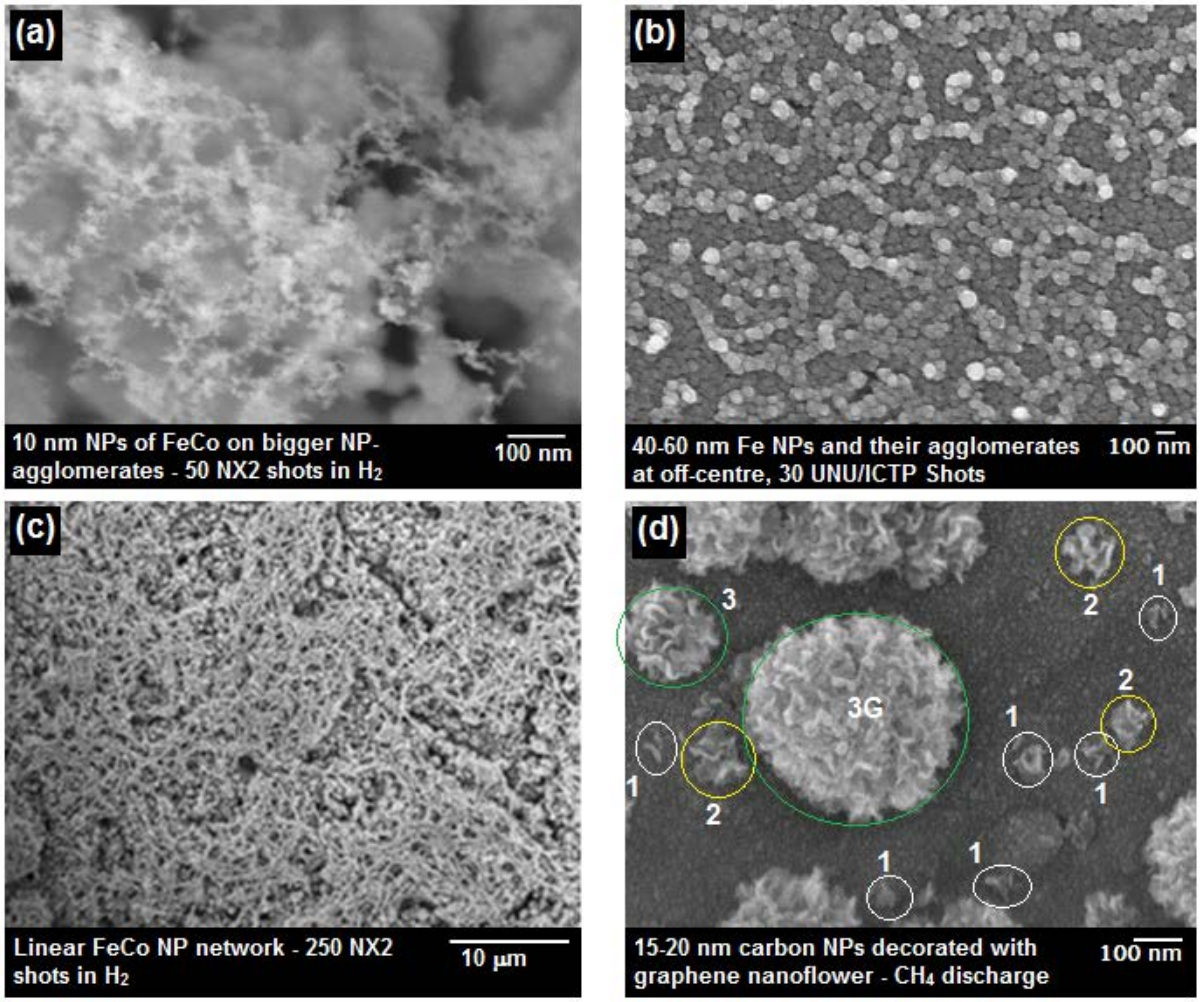

Figure 7. Synthesis of 0-, 1-, 2- and 3- dimensional nanostructures using DPF devices.

(ii) The comparison of FeCo NPs deposited at two different angular positions of 18 and 36 degrees with respect to anode axis shows that for similar number of deposition shots the NPs grown at higher angular position are smaller in size. This can be attributed to essentially forward-directed ablated material plume [123] from the anode top which results in decrease in ablated material flux with the increase in angle with respect to anode axis.

(iii) The average size of NPs decreases with the increase in ambient operating gas pressure. This is evident in the SEM image sequence shown in Figure 8(i-l) for CoPt NP deposition using NX2 DPF device using 25 deposition shots at deposition distance of 25 cm. The average CoPt NP size was found to decrease from about 35 nm for 4 mbar deposition to about 10 nm for deposition done at 8 mbar [128]. The average thickness of CoPt thin film was also found to decrease from about 58 nm for 4 mbar to about 22 nm for 8 mbar deposition. The decrease in NP size as well as film thickness with increasing filling gas pressure is due to two factors: (i) beyond certain operating gas pressure, the focusing efficiency decreases with the increase in filling gas pressure resulting in lesser ablated material from the anode target with lower kinetic

energies, and (ii) with the increase in ambient gas pressure, the collision frequency between the ablation material plume and the ambient gas will increase, which causes the ablated material scatter more and also to lose more energy during their movement from the anode to the substrate.

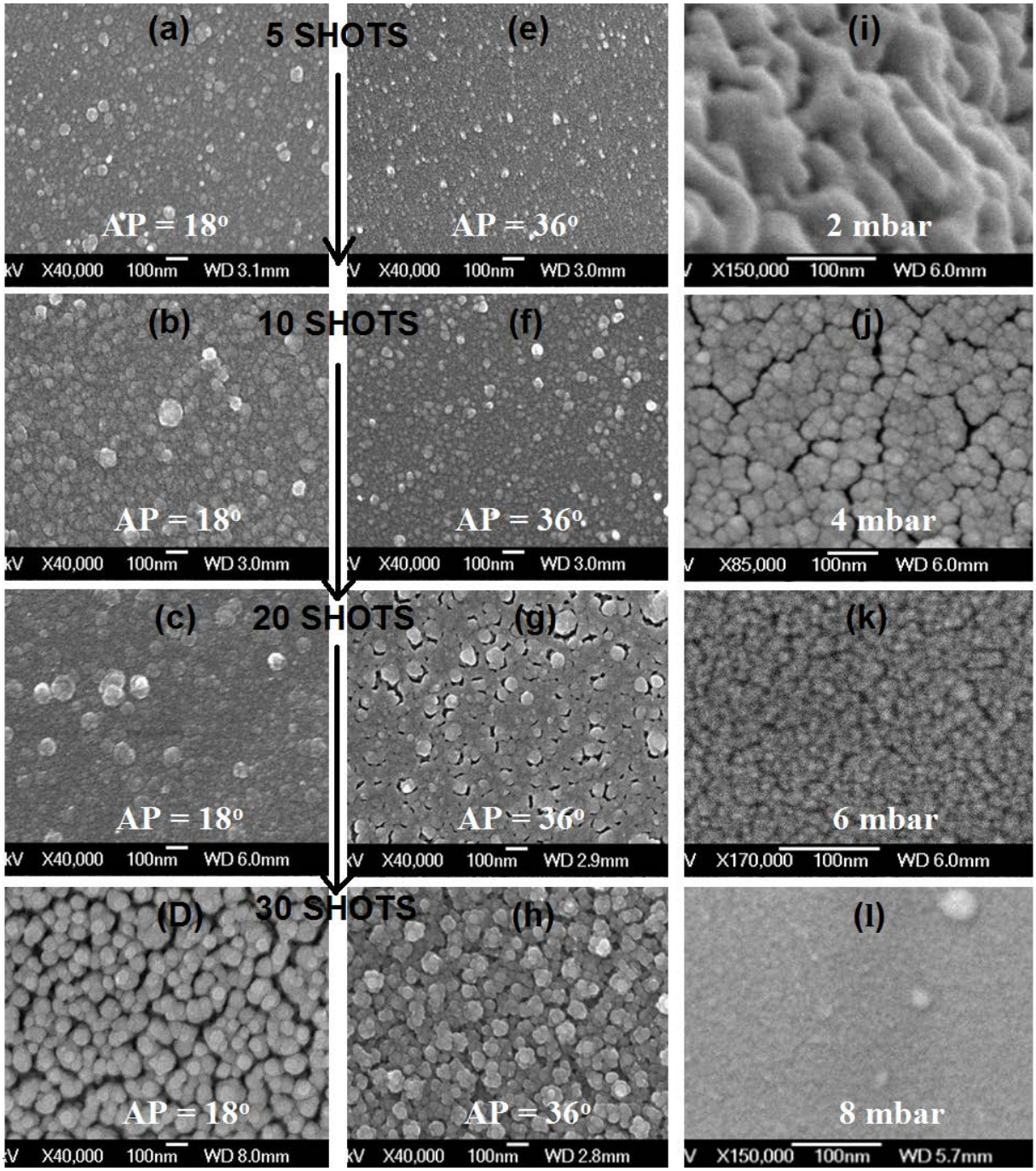

Figure 8. FeCo NPs using different number of DPF shots: (a-d) at angular position (AP) of 18°, and (e-h) at AP of 36° with respect to another. Other operating parameters of DPF devices such as charging voltage, ambient pressure, distance of deposition etc were kept fixed. (i-l) CoPt NPs synthesis with increase filling gas pressure while keeping other parameters fixed.

(iv) The nature of target material ablation, whose thin film is deposited using the setup C1, C3 and C4 of DPF shown in Figure 6, is quite similar to that of PLD as both are pulsed processes and use concentrated flux of energy to ablate the material. The only difference is that instead of using the concentrated flux of laser light energy used in PLD, a complex mix of pulsed energetic electrons/ions and hot-dense plasma is used in DPF device for material ablation. In both cases, PLD and DPF based ablation, the ablated material plume is also forward directed (normal to the target surface) with material flux being highest along the plume centre gradually decreasing radially outward. The DPF device, therefore, suffers from the criticism of non-uniform depositions at the substrate. However, with the availability of 10 Hz or higher repetition rate DPF systems [148-150] one can simply implement the off-axis rotation substrate strategy normally used in PLD device to achieve uniform thin film depositions.

(v) The DPF devices, compared to PLD system, have shown to have significantly higher material ablation rates and hence have thin film deposition rates. For example, the average deposition rate of CoPt thin film was about 1.78 nm/shot for NX2 plasma focus device operating at 880 J at 6 mbar hydrogen ambience at the substrate distance of 25 cm from the anode top [128] which is more than 30 times higher as compared to that of conventional PLD for similar material such as FePt. Similarly, for ZnO nanostructured thin film deposition rates were found to be about 75 nm per shot giving rise to probability of achieving outstanding deposition rates of about 45 μm/min at 10 Hz repetition rate operation of NX2 DPF device [75]. The higher ablation rate of anode top material actually provide significant amount of material even at large distances of deposition. We have routinely observed that in NX2 plasma focus device we can achieve uniform thin film depositions over one inch substrate disc at the larger deposition distance of 25 cm without using any substrate rotation.

(vi) Most of the depositions conducted in DPF devices are essentially multiple-shot depositions which results in transient processing of the thin film, already been deposited previously, by the instability-accelerated energetic ions and hot-dense decay plasma during the next DPF shot. This results in high packing density in the deposited films as well as simultaneous energetic processing (by transient heating) of thin films during deposition. The extent of transient annealing of the deposited material depends on the distance of deposition as well as on the efficient of DPF shot. This, however, most of the time results in direct crystalline phase formation in thin films deposited using DPF device [121, 122, 125, 127, 130, 132-135] without any need for post deposition annealing.

5. Conclusions

The DPF device has successfully been used by many different research groups across the globe for nanostructured material synthesis using both “bottom-up” and “top-down” approaches. Several thin film deposition configurations, in term of target-substrate orientation and placement and use of different ablative components, have been used in DPF devices for nanostructured material syntheses. Each of the DPF based deposition configurations has its own limitations and disadvantages but based on our extensive experience and survey of results from different groups we conclude that most versatile and efficient for thin film deposition setup is the where the target material (to be ablated) is used either as anode insert or as anode tip, background reactive gas is used in the DPF chamber and the substrate (on which thin film is deposited) is placed downstream either along or at some angle with respect to the anode axis. This setup allows deposition of nanostructured metallic, bi-metallic, carbide, nitride, oxide and composite thin films. The DPF device can also be used synthesis for 0-, 1-, 2- and 3-dim nanostructures proving its immense potential in plasma nanoscience and nanotechnology. The DPF device offers a complex mixture of high energy ions of the filling gas species, immensely hot and dense decaying plasma, fast moving ionization wavefront and a strong shockwave that provides a unique plasma and physical/chemical environment that is completely unheard of in any other conventional plasma based deposition or processing facility making it a novel and versatile high energy density pulsed plasma device with immense potential for Plasma Nanotechnology.

Acknowledgement
The author wish to acknowledge research collaborations and scientific discussions with many of his colleagues, collaborators and past PhD students. Financial support from NIE and NTU for various research projects and IAEA research contract is also gratefully acknowledged.

References
1. Mather, J.W., *Formation of a high-density deuterium plasma focus.* Physics of Fluids, 1965. **8**(2): p. 366-&.
2. Filippov, N.V., T.I. Filippova, and V.P. Vinogradov, *Dense, high-temperature plasma in a noncylindrical Z-pinch.* Nuclear Fusion, 1962: p. 577-587.
3. Lee, J.H., et al., *Neutron production mechanism in a plasma focus.* Physics of Fluids, 1971. **14**(10): p. 2210.
4. Schonbach, K.H., L. Michel, and H. Fischer, *Correlation of soft x-ray with hard radiation and neutron emission in 1 kJ plasma focus device.* Applied Physics Letters, 1974. **25**(10): p. 547-549.
5. Oppenländer, T., et al., *The Plasma Focus Current in the Compresion Phase.* Plasma Physics, 1977. **19**: p. 1075.
6. Gullickson, R.L. and H.L. Sahlin, *Measurements of high-energy deuterons in the plasma-focus device.* Journal of Applied Physics, 1978. **49**(3): p. 1099-1105.
7. Bernard, A., et al., Nuclear Instruments & Methods, 1977: p. 191-218.
8. Tendys, J., *Internal report of Australian Atomic Energy Commission*, L.H. Research Establishment, Australia, Editor 1976.
9. Krompholz, H., et al., *A scaling law for plasma-focus devices.* Physics Letters A, 1981. **82**(2): p. 82-84.
10. Lee, S. and A. Serban, *Dimensions and lifetime of the plasma focus pinch.* IEEE Transactions on Plasma Science, 1996. **24**(3): p. 1101-1105.
11. Lee, S. and S.H. Saw, *Neutron scaling laws from numerical experiments.* Journal of Fusion Energy, 2008. **27**: p. 292-295.
12. Krishnan, M., *The Dense Plasma Focus: A Versatile Dense Pinch for Diverse Applications.* Ieee Transactions on Plasma Science, 2012. **40**(12): p. 3189-3221.
13. Rager, J.P., ed. *Uncoventional Approach to Fusion*. ed. B. Brunelli and G. Leotta1982, Plenum: New York. 157.
14. Korzhavin, V.M., ed. *Unconventional approach to fusion*. ed. B. Brunelli and G. Leotta1982, Plenum: New York.
15. Gratton, R., A.R. Piriz, and J.O. Pouzo, Nuclear Fusion, 1986. **26**: p. 483.
16. Dyachenk.Vp and Imshenni.Vs, *Plasma focus and neutron emission mechanism in a Z-pinch.* Soviet Physics Jetp-Ussr, 1969. **29**(5): p. 947-&.
17. Shomo, L.P., J.H. Lee, and K.H. Kim, *Dependence of neutron fluence anisotropy on neutron yied of a plasma focus.* Bulletin of the American Physical Society, 1970. **15**(11): p. 1463-&.
18. Bernstein, M. and F. Hai, *Evidence for nonthermonuclear neutron production in a plasma focus discharge.* Physics Letters A, 1970. **A 31**(6): p. 317-&.
19. Lee, J.H., L.P. Shomo, and K.H. Kim, *Anisotropy of neutron fluence from a plasma focus.* Physics of Fluids, 1972. **15**(12): p. 2433-2438.
20. Pecorella, F., et al., *Time and space resolved neutron measurements on a dense-plasma focus.* Physics of Fluids, 1977. **20**(4): p. 675-682.
21. Cloth, P. and H. Conrads, *Neutronics of a dense-plasma focus - Investigation of a fusion plasma* Nuclear Science and Engineering, 1977. **62**(4): p. 591-600.
22. Zucker, O., et al., *Plasma focus as a large fluence neutron source.* Nuclear Instruments & Methods, 1977. **145**(1): p. 185-190.

23. *Intergrated approach to dense magnetized plasma applications in nuclear fusion technology* in *Report of Coordinated Research Project 2007-2011*2013, International Atomic Energy Agency: Vienna.
24. *Investigations on Materials under High Repetition and Intense Fusion Pulses*. http://cra.iaea.org/crp/project/ProjectDetail?projectId=1754].
25. Zhang, T., et al., *Optimization of a plasma focus device as an electron beam source for thin film deposition.* Plasma Sources Science & Technology, 2007. **16**(2): p. 250-256.
26. Patran, A., et al., *A magnetic electron analyzer for plasma focus electron energy distribution studies.* Journal of Fusion Energy, 2006. **25**(1-2): p. 57-66.
27. Zakaullah, M., et al., *Correlation study of ion, electron and X-ray emission from argon focus plasma.* Physica Scripta, 1998. **57**(1): p. 136-141.
28. Raspa, V., et al., *Plasma focus as a powerful hard x-ray source for ultrafast imaging of moving metallic objects.* Brazilian Journal of Physics, 2004. **34**(4B): p. 1696-1699.
29. Zakaullah, M., et al., *Characteristics of x-rays from a plasma focus operated with neon gas.* Plasma Sources Science & Technology, 2002. **11**(4): p. 377-382.
30. Bhuyan, H., et al., *Comparative study of soft x-ray emission characteristics in a low energy dense plasma focus device.* Journal of Applied Physics, 2004. **95**(6): p. 2975-2981.
31. Barbaglia, M., et al., *Experimental study of the hard x-ray emissions in a plasma focus of hundreds of Joules.* Plasma Physics and Controlled Fusion, 2009. **51**(4): p. 045001.
32. Zhang, T., et al., *Current sheath curvature correlation with the neon soft x-ray emission from plasma focus device.* Plasma Sources Science & Technology, 2005. **14**(2): p. 368-374.
33. Bhuyan, H., et al., *Analysis of nitrogen ion beam produced in dense plasma focus device using Faraday Cup.* Indian Journal of Pure & Applied Physics, 2001. **39**(11): p. 698-703.
34. Kelly, H., et al., *Analysis of the nitrogen ion beam generated in a low-energy plasma focus device by a Faraday Cup operating in the secondary electron emission mode.* Ieee Transactions on Plasma Science, 1998. **26**(1): p. 113-117.
35. Heo, H. and D.K. Park, *Measurement of argon ion beam and X-ray energies in a plasma focus discharge.* Physica Scripta, 2002. **65**(4): p. 350-355.
36. Szydlowski, A., et al., *Measurements of fast ions and neutrons emitted from PF-1000 plasma focus device.* Vacuum, 2004. **76**(2-3): p. 357-360.
37. Gribkov, V.A., et al., *Plasma dynamics in the PF-1000 device under full-scale energy storage: II. Fast electron and ion characteristics versus neutron emission parameters and gun optimization perspectives.* Journal of Physics D-Applied Physics, 2007. **40**(12): p. 3592-3607.
38. Moreno, J., et al., *Preliminary Studies of Ions Emission in a Small Plasma Focus Device of Hundreds of Joules*, in *Dense Z-Pinches*, D.A. Hammer and B.R. Kusse, Editors. 2009. p. 215-218.
39. Rapezzi, L., et al., *Development of a mobile and repetitive plasma focus.* Plasma Sources Science & Technology, 2004. **13**(2): p. 272-277.
40. Tartari, A., et al., *Improvement of calibration assessment for gold fast-neutron activation analysis using plasma focus device.* Measurement Science & Technology, 2002. **13**: p. 939-945.
41. Beckner, E.H., *Production and diagnostic measurements of kilovolt high-density deuterium, helium and neon plasmas.* Journal of Applied Physics, 1966. **37**(13): p. 4944-&.
42. Tan, T.L., et al., *Characterization of chemically amplified resist for X-ray lithography by Fourier transform infrared spectroscopy.* Thin Solid Films, 2006. **504**(1-2): p. 113-116.
43. Kato, Y. and S.H. Be, *Generation of soft x-ray using a rare gas-hydrogen plasma focus and its application to x-ray lithography.* Applied Physics Letters, 1986. **48**(11): p. 686-688.
44. Gribkov, V.A., et al., *Operation of NX2 dense plasma focus device with argon filling as a possible radiation source for micro-machining.* IEEE Transactions on Plasma Science, 2002. **30**(3): p. 1331-1338.

45. Kalaiselvi, S.M.P., et al., *Optimization of neon soft X-rays emission from 200 J fast miniature dense plasma focus device: A potential source for soft X-ray lithography.* Physics Letters A, 2013. **377**(18): p. 1290-1296.
46. Petr, R., et al., *Performance summary on a high power dense plasma focus x-ray lithography point source producing 70 nm line features in AlGaAs microcircuits.* Review of Scientific Instruments, 2004. **75**(8): p. 2551-2559.
47. Kato, Y., et al., *Plasma focus x-ray source for lithography.* Journal of Vacuum Science & Technology B, 1988. **6**(1): p. 195-198.
48. Bogolyubov, E.P., et al., *A powerful soft X-ray source for X-ray lithography based on plasma focusing.* Physica Scripta, 1998. **57**(4): p. 488-494.
49. Rawat, R.S., et al., *Soft X-ray imaging using a neon filled plasma focus X-ray source.* Journal of Fusion Energy, 2004. **23**(1): p. 49-53.
50. Hussain, S., et al., *Low energy plasma focus as an intense X-ray source for radiography.* Plasma Science & Technology, 2004. **6**(3): p. 2296-2300.
51. Hussain, S., et al., *Plasma focus as a possible x-ray source for radiography.* Plasma Sources Science & Technology, 2005. **14**(1): p. 61-69.
52. Moreno, C., et al., *Plasma-focus-based tabletop hard x-ray source for 50 ns resolution introspective imaging of metallic objects through metallic walls.* Applied Physics Letters, 2006. **89**(9).
53. Raspa, V., et al., *Effective hard x-ray spectrum of a tabletop Mather-type plasma focus optimized for flash radiography of metallic objects.* Journal of Applied Physics, 2007. **102**(12).
54. Di Lorenzo, F., et al., *Hard x-ray source for flash radiography based on a 2.5 kJ plasma focus.* Journal of Applied Physics, 2007. **102**(3).
55. Castillo, F., et al., *High contrast radiography using a small dense plasma focus.* Applied Physics Letters, 2008. **92**: p. 051502.
56. Gribkov, V.A., *Current and perspective applications of Dense Plasma Focus devices*, in *Plasma and Fusion Science*, C. Varandas and C. Silva, Editors. 2008. p. 51-64.
57. Verma, R., et al., *Miniature Plasma Focus Device as a Compact Hard X-Ray Source for Fast Radiography Applications.* IEEE Transactions on Plasma Science, 2010. **38**(4): p. 652-657.
58. Roshan, M.V., et al., *Short-Lived PET Radioisotope Production in a Small Plasma Focus Device.* IEEE Transactions on Plasma Science, 2010. **38**(12): p. 3393-3397.
59. Brzosko, J.S., et al., *Breeding 10(10)/s radioactive nuclei in a compact plasma focus device*, in *Application of Accelerators in Research and Industry*, J.L. Duggan and I.L. Morgan, Editors. 2001, Amer Inst Physics: Melville. p. 277-280.
60. Sumini, M., et al., *Preliminary design of a 150kJ repetitive plasma focus for the production of 18-F.* Nuclear Instruments & Methods in Physics Research Section a-Accelerators Spectrometers Detectors and Associated Equipment, 2006. **562**(2): p. 1068-1071.
61. Talaei, A., S.M.S. Kiai, and A.A. Zaeem, *Effects of admixture gas on the production of F-18 radioisotope in plasma focus devices.* Applied Radiation and Isotopes, 2010. **68**(12): p. 2218-2222.
62. Shirani, B., F. Abbasi, and M. Nikbakht, *Production of N-13 by C-12(d,n)N-13 reaction in a medium energy plasma focus.* Applied Radiation and Isotopes, 2013. **74**: p. 86-90.
63. Feugeas, J.N., et al., *Nitrogen implantation of AISI 304 stainless steel with a coaxial plasma gun.* Journal of Applied Physics, 1988. **64**(5): p. 2648-2651.
64. Rawat, R.S., et al., *Crystallization of an amorphous lead zirconate titanate thin film with a dense plasma focus device.* Physical Review B, 1993. **47**(9): p. 4858-4862.
65. Kant, C.R., M.P. Srivastava, and R.S. Rawat, *Thin carbon film deposition using energetic ions of a dense plasma focus.* Physics Letters A, 1997. **226**(3-4): p. 212-216.
66. Ostrikov, K. and A.B. Murphy, *Plasma-aided nanofabrication: where is the cutting edge?* Journal of Physics D-Applied Physics, 2007. **40**(8): p. 2223-2241.

67. Ostrikov, K., U. Cvelbar, and A.B. Murphy, *Plasma nanoscience: setting directions, tackling grand challenges.* Journal of Physics D-Applied Physics, 2011. **44**(17).
68. Meyyappan, M., *Plasma nanotechnology: past, present and future.* Journal of Physics D-Applied Physics, 2011. **44**(17).
69. Shiratani, M., et al., *Nano-factories in plasma: present status and outlook.* Journal of Physics D-Applied Physics, 2011. **44**(17).
70. Soto, L., *New trends and future perspectives on plasma focus research.* Plasma Physics and Controlled Fusion, 2005. **47**: p. A361-A381.
71. Committee on High Energy Density Plasma Physics, P.S.C., National Research Council *Frontiers in High Energy Density Physics: The X-Games of Contemporary Science*2003: National Academies Press. 176.
72. Hassan, S.M., et al., *Pinching evidences in a miniature plasma focus with fast pseudospark switch.* Plasma Sources Science & Technology, 2006. **15**(4): p. 614-619.
73. Bernard, A., et al., *Experimental studies of plasma focus and evidence for non-thermal processes.* Physics of Fluids, 1975. **18**(2): p. 180-194.
74. Bernard, A., et al., *Dense plasma focus - high intensity neutron source.* Nuclear Instruments & Methods, 1977. **145**(1): p. 191-218.
75. Rawat, R.S., *High-Energy-Density Pinch Plasma: A Unique Nonconventional Tool for Plasma Nanotechnology.* Ieee Transactions on Plasma Science, 2013. **41**(4): p. 701-715.
76. Lee, S., et al., *Numerical experiments on plasma focus neon soft x-ray scaling.* Plasma Physics and Controlled Fusion, 2009. **51**(10): p. 105013.
77. Toepfer, A.J., D.R. Smith, and E.H. Beckner, *Ion heating in dense plasma focus.* Bulletin of the American Physical Society, 1969. **14**(11): p. 1013-&.
78. Qi, N., et al., *Space and time resolved electron density and current measurements in a dense plasma focus z-pinch.* Ieee Transactions on Plasma Science, 1998. **26**(4): p. 1127-1137.
79. Choi, P., et al., *Characterization of self-generated intense electron beams in a plasma focus.* Laser and Particle Beams, 1990. **8**(3): p. 469-476.
80. Roshan, M.V., et al., *Magnetic spectrometry of high energy deuteron beams from pulsed plasma system.* Plasma Physics and Controlled Fusion, 2010. **52**(8): p. 085007.
81. Sanchez, G. and J. Feugeas, *The thermal evolution of targets under plasma focus pulsed ion implantation.* Journal of Physics D-Applied Physics, 1997. **30**(6): p. 927-936.
82. Lin, J.J., et al., *FePt nanoparticle formation with lower phase transition temperature by single shot plasma focus ion irradiation.* Journal of Physics D-Applied Physics, 2008. **41**(13).
83. Lee, S. and S.H. Saw, *Plasma focus ion beam fluence and flux-Scaling with stored energy.* Physics of Plasmas, 2012. **19**(11).
84. Lee, S. and S.H. Saw, *Plasma focus ion beam fluence and flux-For various gases.* Physics of Plasmas, 2013. **20**(6).
85. Gupta, R. and M.P. Srivastava, *Carbon ion implantation on titanium for TiC formation using a dense plasma focus device.* Plasma Sources Science & Technology, 2004. **13**(3): p. 371-374.
86. Hassan, M., et al., *Nitriding of titanium by using an ion beam delivered by a plasma focus.* Journal of Physics D-Applied Physics, 2007. **40**(3): p. 769-777.
87. Hassan, M., et al., *Synthesis of nanocrystalline multiphase titanium oxycarbide (TiCxOy) thin films by UNU/ICTP and NX2 plasma focus devices.* Applied Physics a-Materials Science & Processing, 2008. **90**(4): p. 669-677.
88. Hassan, M., et al., *Dense plasma focus ion-based titanium nitride coating on titanium.* Nuclear Instruments & Methods in Physics Research Section B-Beam Interactions with Materials and Atoms, 2009. **267**(11): p. 1911-1917.
89. Bhuyan, H., et al., *High energy ion beam irradiation on titanium substrate in a pulsed plasma device operating with methane.* Journal of Physics D-Applied Physics, 2009. **42**(20): p. 205207.

90. Valipour, M., et al., *Increasing of Hardness of Titanium Using Energetic Nitrogen Ions from Sahand as a Filippov Type Plasma Focus Facility*. Journal of Fusion Energy, 2012. **31**(1): p. 65-72.
91. Gribkov, V.A., et al., *Interaction of high temperature deuterium plasma streams and fast ion beams with stainless steels in dense plasma focus device.* Journal of Physics D-Applied Physics, 2003. **36**(15): p. 1817-1825.
92. Shafiq, M., et al., *Dense plasma focus-assisted nitriding of AISI-304.* Radiation Effects and Defects in Solids, 2008. **163**(9): p. 729-736.
93. Feugeas, J., et al., *Austenite modification of AISI 316L SS by pulsed nitrogen ion beams generated in dense plasma focus discharges.* Surface & Coatings Technology, 2010. **204**(8): p. 1193-1199.
94. Sadiq, M., et al., *Amorphization of silicon by ion irradiation in dense plasma focus.* Physics Letters A, 2006. **352**(1-2): p. 150-154.
95. Sadiq, M., et al., *Nitrogen ion implantation of silicon in dense plasma focus.* Nuclear Instruments & Methods in Physics Research Section B-Beam Interactions with Materials and Atoms, 2006. **252**(2): p. 219-224.
96. Bhuyan, H., et al., *Effect of high energy ion irradiation on silicon substrate in a pulsed plasma device.* Applied Surface Science, 2007. **254**(1): p. 197-200.
97. Bhuyan, H., et al., *Formation of hexagonal silicon carbide by high energy ion beam irradiation on Si(100) substrate.* Journal of Physics D-Applied Physics, 2007. **40**(1): p. 127-131.
98. Wang, Z.R., et al., *Preparation of silicon carbide film by a plasma focus device.* Physics Letters A, 2008. **372**(48): p. 7179-7182.
99. Jabbar, S., et al., *Carbonitriding of silicon using plasma focus device.* Journal of Vacuum Science & Technology A, 2009. **27**(2): p. 381-387.
100. Ahmad, M., S. Al-Hawat, and M. Akel, *Porous Structure Formation on Silicon Surface Treated by Plasma Focus Device.* Journal of Fusion Energy, 2013. **32**(4): p. 471-478.
101. Roshan, M.V., et al., *High energy ions and energetic plasma irradiation effects on aluminum in a Filippov-type plasma focus.* Applied Surface Science, 2008. **255**(5): p. 2461-2465.
102. Rad, Z.S., M. Shahriari, and F.A. Davani, *Investigation of Spatial Distribution of Hydrogen and Argon Ions and Effects of them on Aluminum Samples in a 2.5 kJ Mater Type Plasma Focus Device.* Journal of Fusion Energy, 2011. **30**(5): p. 358-366.
103. Afrashteh, M. and M. Habibi, *Study of Dense Nitrogen Plasma Irradiation of Aluminum Targets by APF Plasma Focus Device.* Journal of Fusion Energy, 2012. **31**(3): p. 223-226.
104. Rico, L., et al., *Crystallization of amorphous zirconium thin film using ion implantation by a plasma focus of 1 kJ.* Applied Surface Science, 2007. **254**(1): p. 193-196.
105. Khan, I.A., et al., *Nitridation of zirconium using energetic ions from plasma focus device.* Thin Solid Films, 2008. **516**(23): p. 8255-8263.
106. Khan, I.A., et al., *Synthesis of zirconium oxynitride (ZrON) nanocomposite films on zirconium substrate by dense plasma focus device.* International Journal of Modern Physics B, 2008. **22**(23): p. 3941-3955.
107. Khan, I.A., et al., *Synthesis of nano-crystalline zirconium aluminium oxynitride (ZrAlON) composite films by dense plasma Focus device.* Applied Surface Science, 2009. **255**(12): p. 6132-6140.
108. Khan, I.A., et al., *Deposition of zirconium carbonitride composite films using ion and electron beams emitted from plasma focus device.* Nuclear Instruments & Methods in Physics Research Section B-Beam Interactions with Materials and Atoms, 2010. **268**(13): p. 2228-2234.
109. Murtaza, G., et al., *Carburizing of zirconium using a low energy Mather type plasma focus.* Surface & Coatings Technology, 2011. **205**(8-9): p. 3012-3019.
110. Khan, I.A., et al., *Deposition of alumina stabilized zirconia at room temperature by plasma focus device.* Applied Surface Science, 2014. **288**: p. 304-312.

111. Mohanty, S.R., et al., *Energetic ion irradiation of American diamond in a plasma focus device and characterization of irradiated material.* Nuclear Instruments & Methods in Physics Research Section B-Beam Interactions with Materials and Atoms, 2006. **243**(1): p. 113-118.
112. Bhuyan, M., et al., *Plasma focus assisted damage studies on tungsten.* Applied Surface Science, 2013. **264**: p. 674-680.
113. Wong, D., et al., *Soft X-ray optimization studies on a dense plasma focus device operated in neon and argon in repetitive mode.* IEEE Transactions on Plasma Science, 2004. **32**(6): p. 2227-2235.
114. Pan, Z.Y., et al., *Nanostructuring of FePt thin films by plasma focus device: pulsed ion irradiation dependent phase transition and magnetic properties.* Applied Physics a-Materials Science & Processing, 2009. **96**(4): p. 1027-1033.
115. Pan, Z.Y., et al., *Lowering of L1(0) phase transition temperature of FePt thin films by single shot H+ ion exposure using plasma focus device.* Thin Solid Films, 2009. **517**(8): p. 2753-2757.
116. Mohanty, S.R., et al., *Self-organized transformation to polyaniline nanowires by pulsed energetic electron irradiation in a plasma focus device.* Physics Letters A, 2009. **373**(22): p. 1962-1966.
117. Lee, S., et al., *A simple facility for the teaching of plasma dynamics and plasma nuclear fusion.* American Journal of Physics, 1988. **56**(1): p. 62-68.
118. Alexander, D.E., et al., Applied Physics Letters, 1993. **62**: p. 1597.
119. Liang, L., et al., *Direct assembly of large arrays of oriented conducting polymer nanowires.* Angewandte Chemie-International Edition, 2002. **41**(19): p. 3665-3668.
120. Patran, A., et al., *Spectral study of the electron beam emitted from a 3 kJ plasma focus.* Plasma Sources Science & Technology, 2005. **14**(3): p. 549-560.
121. Rawat, R.S., et al., *Room temperature deposition of titanium carbide thin films using dense plasma focus device.* Surface & Coatings Technology, 2001. **138**(2-3): p. 159-165.
122. Rawat, R.S., et al., *Deposition of titanium nitride thin films on stainless steel - AISI 304 substrates using a plasma focus device.* Surface & Coatings Technology, 2003. **173**(2-3): p. 276-284.
123. Soh, L.Y., et al., *Shadowgraphic studies of DLC film deposition process in dense plasma focus device.* IEEE Transactions on Plasma Science, 2004. **32**(2): p. 448-455.
124. Gupta, R., et al., *Deposition of nanosized grains of ferroelectric lead zirconate titanate on thin films using dense plasma focus.* Journal of Physics D-Applied Physics, 2004. **37**(7): p. 1091-1094.
125. Rawat, R.S., et al., *Nano-structured Fe thin film deposition using plasma focus device.* Applied Surface Science, 2006. **253**(3): p. 1611-1615.
126. Zhang, T., et al., *Characteristics of FeCo nano-particles synthesized using plasma focus.* Journal of Physics D-Applied Physics, 2006. **39**(10): p. 2212-2219.
127. Rawat, R.S., et al., *Nano-phase titanium dioxide thin film deposited by repetitive plasma focus: Ion irradiation and annealing based phase transformation and agglomeration.* Applied Surface Science, 2008. **255**(5): p. 2932-2941.
128. Pan, Z.Y., et al., *Nanostructured magnetic CoPt thin films synthesis using dense plasma focus device operating at sub-kilojoule range.* Journal of Physics D-Applied Physics, 2009. **42**(17): p. 175001.
129. Malhotra, Y., et al., *Extremely non-equilibrium synthesis of luminescent zinc oxide nanoparticles through energetic ion condensation in a dense plasma focus device.* Journal of Physics D-Applied Physics, 2009. **42**(15): p. 155202.
130. Ghareshabani, E., et al., *Synthesis of nanostructured multiphase Ti(C,N)/a-C films by a plasma focus device.* Nuclear Instruments & Methods in Physics Research Section B-Beam Interactions with Materials and Atoms, 2010. **268**(17-18): p. 2777-2784.

131. Ghareshabani, E., et al., *Low energy repetitive miniature plasma focus device as high deposition rate facility for synthesis of DLC thin films.* Applied Surface Science, 2010. **256**(16): p. 4977-4983.
132. Pan, Z.Y., et al., *Miniature plasma focus as a novel device for synthesis of soft magnetic FeCo thin films.* Physics Letters A, 2010. **374**(8): p. 1043-1048.
133. Macharaga, G., et al., *TiO2 Nano-cluster Thin Films by Dense Plasma Focus and Ion Implantation Effect on its Photocatalytic Activity*. Journal of Advanced Oxidation Technologies, 2011. **14**(2): p. 308-313.
134. Etaati, G.R., et al., *Deposition of tungsten nitride on stainless steel substrates using plasma focus device*. Nuclear Instruments & Methods in Physics Research Section B-Beam Interactions with Materials and Atoms, 2011. **269**(10): p. 1058-1062.
135. Hosseinnejad, M.T., et al., *Deposition of tungsten nitride thin films by plasma focus device at different axial and angular positions.* Applied Surface Science, 2011. **257**(17): p. 7653-7658.
136. Javadi, S., et al., *Deposition of Chromium Thin Films on Stainless Steel-304 Substrates Using a Low Energy Plasma Focus Device.* Journal of Fusion Energy, 2012. **31**(3): p. 242-248.
137. Ngoi, S.K., et al., *Formation of Nano-Crystalline Phase in Hydrogenated Amorphous Silicon Thin Film by Plasma Focus Ion Beam Irradiation.* Journal of Fusion Energy, 2012. **31**(1): p. 96-103.
138. Hosseinnejad, M.T., et al., *Using Mather-Type Plasma Focus Device for Fabrication of Tungsten Thin Films.* Journal of Fusion Energy, 2012. **31**(5): p. 426-431.
139. Umar, Z.A., et al., *Hard TiCx/SiC/a-C:H nanocomposite thin films using pulsed high energy density plasma focus device.* Nuclear Instruments & Methods in Physics Research Section B-Beam Interactions with Materials and Atoms, 2013. **301**: p. 53-61.
140. Borthakur, T.K., et al., *Surface hardening of high carbon steel by plasma focus nitriding.* Surface Engineering, 1999. **15**(1): p. 55-58.
141. Sadiq, M., et al., *The nitriding of aluminium by dense plasma focus.* Plasma Sources Science & Technology, 2006. **15**(3): p. 295-301.
142. Shafiq, M., et al., *Pulsed ion beam-assisted carburizing of titanium in methane discharge.* Chinese Physics B, 2010. **19**(1): p. 012801.
143. Kovaleski, S.D., et al., *Electron beam ablation of materials.* Journal of Applied Physics, 1999. **86**(12): p. 7129-7138.
144. Stark, R., et al., *Pseudospark produced pulsed electron beam for material processing.* Ieee Transactions on Plasma Science, 1995. **23**(3): p. 258-264.
145. Strikovski, M. and K.S. Harshavardhan, *Parameters that control pulsed electron beam ablation of materials and film deposition processes.* Applied Physics Letters, 2003. **82**(6): p. 853-855.
146. Happy, et al., *Effect of deposition parameters on morphology and size of FeCo nanoparticles synthesized by pulsed laser ablation deposition.* Applied Surface Science, 2006. **252**(8): p. 2806-2816.
147. Lin, J.J., et al., *Effects of target-substrate geometry and ambient gas pressure on FePt nanoparticles synthesized by pulsed laser deposition.* Applied Surface Science, 2009. **255**(8): p. 4372-4377.
148. Lee, S., et al., *High rep rate high performance plasma focus as a powerful radiation source.* IEEE Transactions on Plasma Science, 1998. **26**(4): p. 1119-1126.
149. Soto, L., et al., *Nanofocus of tenth of joules and a portable plasma focus of few joules for field applications*, in *Dense Z-Pinches*, D.A. Hammer and B.R. Kusse, Editors. 2009. p. 219-222.
150. Verma, R., et al., *High Performance High Repetition Rate Miniature Plasma Focus Device: Record Time Averaged Neutron Yield at 200 J with Enhanced Reproducibility.* Journal of Fusion Energy, 2013. **32**(1): p. 2-10.